AIP | Advances

Phonon scattering limited performance of monolayer MoS2 and WSe2 n-MOSFET

Amretashis Sengupta, Anuja Chanana, and Santanu Mahapatra

Citation: AIP Advances **5**, 027101 (2015); doi: 10.1063/1.4907697
View online: http://dx.doi.org/10.1063/1.4907697
View Table of Contents: http://scitation.aip.org/content/aip/journal/adva/5/2?ver=pdfcov
Published by the AIP Publishing

Phonon scattering limited performance of monolayer MoS_2 and WSe_2 n-MOSFET

Amretashis Sengupta,[1,a] Anuja Chanana,[2] and Santanu Mahapatra[2]
[1]*School of VLSI Technology, Indian Institute of Engineering Science and Technology, Shibpur, Howrah-711103, India*
[2]*Nano-Scale Device Research Laboratory, Department of Electronic Systems Engineering, Indian Institute of Science, Bangalore-560012, India*

(Received 8 December 2014; accepted 24 January 2015; published online 5 February 2015)

In this paper we show the effect of electron-phonon scattering on the performance of monolayer (1L) MoS_2 and WSe_2 channel based n-MOSFETs. Electronic properties of the channel materials are evaluated using the local density approximation (LDA) in density functional theory (DFT). For phonon dispersion we employ the small displacement / frozen phonon calculations in DFT. Thereafter using the non-equilibrium Green's function (NEGF) formalism, we study the effect of electron-phonon scattering and the contribution of various phonon modes on the performance of such devices. It is found that the performance of the WSe_2 device is less impacted by phonon scattering, showing a ballisticity of 83% for 1L-WSe_2 FET for channel length of 10 nm. Though 1L-MoS_2 FET of similar dimension shows a lesser ballisticity of 75%. Also in the presence of scattering there exist a a 21–36% increase in the intrinsic delay time (τ) and a 10–18% reduction in peak transconductance (g_m) for WSe_2 and MoS_2 devices respectively. [http://dx.doi.org/10.1063/1.4907697]

I. INTRODUCTION

Two dimensional (2-D) materials such as the Transition Metal Dichalcogenides (MX_2 : M=Mo, W; X=S, Se, Te) have emerged as a prospective channel material for the post-Si CMOS technology.[1,3–6] Among such MX_2 materials so far the MoS_2 and WSe_2 have been successfully realized into MOS devices experimentally.[1–3] Apart from monolayer flakes of such MX_2 materials, few layers thick MX_2 MOSFET have also been the focus of various device fabrication studies.[7–9]

The role of electron-phonon scattering in such MX_2 layers do have a significant impact on the performance of such 2-D channel MOSFETs.[10–12] Recently Guo *et al*. have shown the effect of phonon scattering in monolayer MoS_2 MOSFETs.[12] According to recent simulations tungsten chalcogenide (e.g. WS_2) FETs are expected to outperform other MX_2 FETs in the ballistic limit.[6] However in the more realistic case, the devices often operate at the quasi-ballistic limit. In this regard it could be of interest to comparatively study the MoS_2 and WSe_2 MOSFET inclusive of the electron-phonon scattering. In this paper we study difference in performance of 1L-MX_2 (hereafter by MX_2 we refer to MoS_2 and WSe_2 only) channel 2-D planar n-MOSFET in the quasi-ballistic regime. The materials properties of the monolayer MX_2 channel are modeled by ab-initio methods. Thereafter using our in-house simulator based on the non-equilibrium Green's function (NEGF) formalism, we calculate the performance parameters of the MX_2 n-MOSFETs. It is found that performance of WSe_2 devices are less impacted by phonon scattering compared to the MoS_2 counterparts.

[a]Corresponding Author: a.sengupta@vlsi.iiests.ac.in

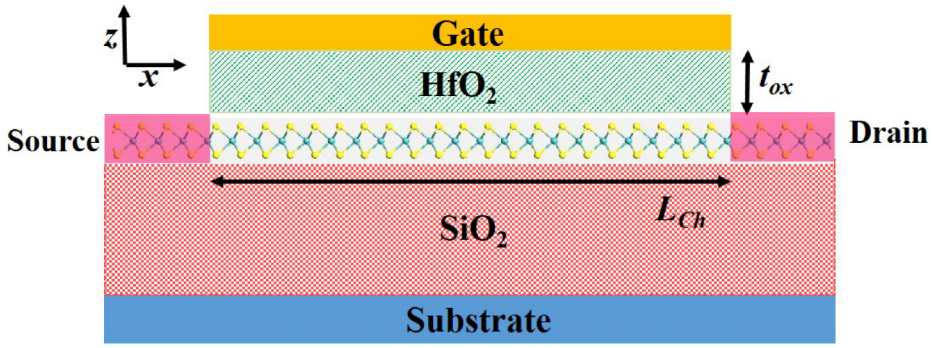

FIG. 1. The device schematic (not to scale) of the n-MOSFET with single layer (1L) MoS_2 or WSe_2 as the channel material.

II. METHODOLOGY

Fig. 1 shows the schematic device structure of the planar 2-D MoS_2 FET considered for our studies. We consider a 1L MoS_2 or WSe_2 as the channel material. As shown in Fig. 1. The 2-D channel is placed over an SiO_2/Si substrate. High-κ HfO_2 of 2.5nm thickness is chosen as the gate dielectric. We consider highly doped (10^{20} /cm^3) n^{++} regions as the source/drain for the n-MOSFET. Such doping concentrations allow for good alignment of the source/drain fermi levels with the conduction band for the monolayer MX_2 FETs.[5,6]

In the first step in our study we evaluate the different properties of the MX_2 channel material e.g. bandstructure, electron effective mass, phonon spectra and phonon density of states, by ab-initio simulations. For this purpose we employ density functional theory(DFT) in QuantumWise ATK.[13] We use a $16 \times 16 \times 1$ Monkhorst-Pack k-grid[15] and employ the Local Density Approximation (LDA) exchange correlation function with the Perdew Zunger(PZ) basis.[16] The DFT simulations are performed by relaxing the structures by optimizing the positions by a Broyden - Fletcher - Goldfarb - Shanno (BFGS)[17] Quasi-Newton optimization method in ATK with maximum force of 0.05 eV/Å. The energy cut-off value in our simulations is set at 75 Hartree.

The phonon dispersion and phonon DOS are calculated in ATK using a supercell based small displacement method also known as the frozen phonon calculations. In this method employing a finite difference scheme the first derivative of the forces are calculated, where the system is displaced by small amounts along each degree of freedom.[10,13] For phonon calculations in ATK we use a $9 \times 9 \times 1$ supercell. 72 small displacements, each of value 0.01Å is applied to the supercell in the x and the y directions. From this the forces are calculated and subsequently the dynamical matrix of the system is found out, which is used in calculating the phonon properties.

Thereafter, we proceed to solve the Poisson and Schrödinger equations self-consistently for our MX_2 FET. The self-consistent solutions are carried out under the Non-Equilibrium Green's Function (NEGF) formalism[12,18] with our in-house NEGF simulator.[19] The electron-phonon interaction in the quasi-ballistic regime is incorporated into our simulator by self-consistent Born approximation method within the framework of NEGF formalism.[12,18] In our solver, we construct the Green's function using an effective mass Hamiltonian H and the energy eigenvalue matrix E of the system along with the self-energy matrix of the system Σ.[20,21]

$$G(E) = [(E + i\emptyset^{+})I - H - \Sigma(E)]^{-1} \tag{1}$$

In (1) I is the identity matrix and $\emptyset^{+}$ is an infinitesimally positive quantity. The self-energy matrix Σ consists of Σ_C for the source and drain contacts and Σ_{Sc} which is the scattering self-energy matrix.

$$\Sigma(E) = \Sigma_C(E) + \Sigma_{Sc}(E) \tag{2}$$

$$\Sigma_C(E) = \Sigma_1(E) + \Sigma_2(E) \tag{3}$$

The spectral density $A(E)$ is expressed as

$$A(E) = i[G(E) - G^{\dagger}(E)] \tag{4}$$

the Green's correlation function for the n-type and p-type carriers exclusively can be expressed as G^n and G^p, and spectral density can also be expressed in terms of these two as[18]

$$A(E) = G^n(E) + G^p(E) \tag{5}$$

The broadening Γ is obtained from the self-energy as

$$\Gamma(E) = i[\Sigma(E) - \Sigma^{\dagger}(E)] \tag{6}$$

in terms of the in-scattering and out-scattering self-energies of the system it takes the form

$$\Gamma(E) = \Sigma^{in}(E) + \Sigma^{out}(E) \tag{7}$$

For electron-phonon scattering we consider G^n, which is found as[18]

$$G^n(E) = G(E)(\Sigma_C^{in}(E) + \Sigma_{Sc}^{in}(E))G^{\dagger}(E) \tag{8}$$

while G^p, which is found as

$$G^p(E) = G(E)(\Sigma_C^{out}(E) + \Sigma_{Sc}^{out}(E))G^{\dagger}(E) \tag{9}$$

In the self-consistent Born approximation approach the in and the out scattering self-energies are evaluated as

$$\Sigma^{in,out} = \Delta^{n,p} G^{n,p} \tag{10}$$

here Δ represents the spin relaxation tensor. The number density of the electrons in a 2-D system of cell volume V_{xy} is

$$n(r) = g_s g_v \frac{1}{V_{xy}} \int_{-\infty}^{+\infty} \frac{G^n(r,E)dE}{2\pi} \tag{11}$$

similarly the number density for holes is given by

$$p(r) = g_s g_v \frac{1}{V_{xy}} \int_{-\infty}^{+\infty} \frac{G^p(r,E)dE}{2\pi} \tag{12}$$

g_s and g_v being the spin and the valley degeneracies, r being the positional co-ordinate. This carrier (electron) density is evaluated self-consistently within the Poisson-Schrodinger solver.

The Green's functions G, $G^{n,p}$ the in and out scattering self energies $\Sigma^{in,out}$ are all evaluated using a recursive algorithm with the self-consistent Born approximation approach, as described in detail by Nikonov *et al.*[18] The drain current is evaluated as[4,19]

$$I_D = \frac{q}{\hbar^2}\sqrt{\frac{m_t k_B T}{2\pi^3}} \int_{-\infty}^{\infty} [F_{-1/2}(\frac{\eta_1 - E_{k,x}}{k_B T}) - F_{-1/2}(\frac{\eta_2 - E_{k,x}}{k_B T})]\Im(E_{k,x})dE \tag{13}$$

m_t being the carrier effective mass in the transverse direction, k_B is Boltzmann constant, T is temperature, $E_{k,x}$ the energy of the conducting level, $F_{-1/2}$ is the Fermi integral of order $-1/2$. η_1 and η_2 are the chemical potentials of the source and drain respectively. $\Im(E)$ is the transmission matrix given as

$$\Im(E) = trace[A_1\Gamma_2] = trace[A_2\Gamma_1] \tag{14}$$

the subscripts 1 and 2 designating the source and the drain contacts. For calculating currents purely ballistic in nature, the scattering self-energy matrix Σ_{Sc} in (2) is considered zero and the calculations for such a case is described in detail by Sengupta *et al.*[19] Among the measured parameters the ballisticity is expressed as a ratio between the drain currents including scattering I_D and the purely

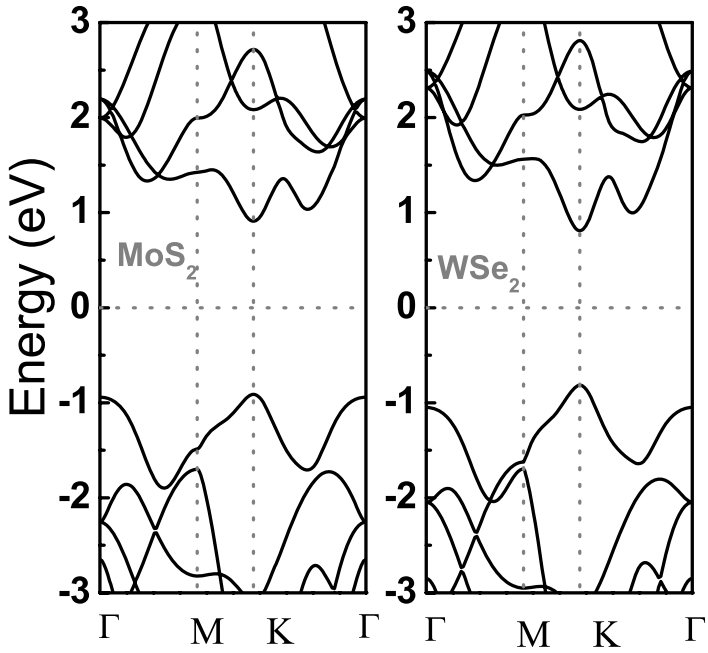

FIG. 2. The bandstructure of single layer MoS_2 and WSe_2.

ballistic drain current $I_{D,Bal}$. The ON current I_{ON} for the devices are calculated at $V_G = V_D = 0.4$ V. The intrinsic delay time τ is expressed as $\tau = (C_{gg} + C_f) \times V_{DD}/I_{ON}$, where C_{gg} is the device gate capacitance expressed as series combination of geometrical oxide capacitance C_{ox} and the channel quantum capacitance C_Q, C_f is the fringing capacitance.[20,21] V_{DD} is the supply voltage (0.4 V).

III. RESULTS AND DISCUSSIONS

Fig. 2 shows the simulated bandstructure of the 1L MX_2 sheets. Our DFT simulations show a direct band gap at the K point of the hexagonal Brillouin zone for both the 1L-MoS_2 and 1L-WSe_2 sheets with band-gap values of 1.82 and 1.62 eV respectively. Such values are agreeable to ab-initio results in recent reports.[14] The effective masses obtained in our studies (Table I) are also consistent with ab-initio simulation results reported elsewhere.[4,6,12]

In Fig. 3, we show the calculated phonon bandstructures for the layered MX_2 sheets under consideration. The in-plane acoustic vibration modes of the MX_2, namely the longitudinal acoustic (LA) and the transverse acoustic (TA) modes have higher energy compared to the out-of plane acoustic mode (ZA). These acoustic phonon modes in MX_2 are clearly separated from the optical phonon modes. The two lowest branches of the optical modes are non-polar (NP) in nature, followed by the transverse optical (TO) and the longitudinal optical (LO) modes. The mode(s) with very low dispersion at energies 50 meV in MoS_2 and 30 meV in WSe_2 are known as the homopolar (HP) modes. Fig. 4 shows the calculated phonon density of states of the monolayer MoS_2 and WSe_2.

Among the different modes we can consider the LA, TA and ZA modes to contribute to acoustic scattering, non-polar optical and TO and HP modes to contribute to the optical phonon

TABLE I. Electron effective masses at the conduction band minima calculated from our DFT simulations.

material	m_l/m_0	m_t/m_0
1L-MoS_2	0.4742	0.4738
1L-WSe_2	0.3376	0.3372

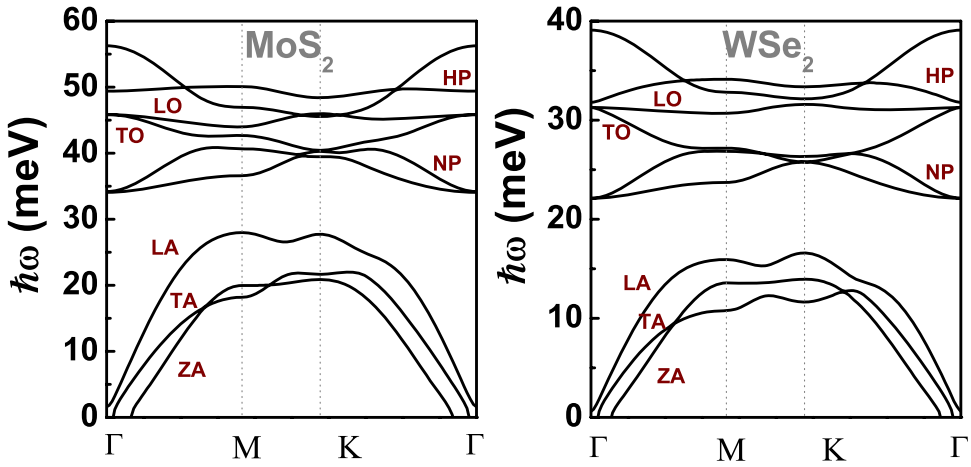

FIG. 3. The phonon dispersion of single layer MoS_2 and WSe_2.

scattering, while the polar LO modes are responsible for the Frölich interaction mechanism of electron-phonon scattering. The phonon energies of the different modes at the CB minima of the electronic bandstructure are considered in order to evaluate the electron-phonon interaction matrix and subsequently the scattering self-energy matrix Σ_S in the channel.[18]

In Fig. 5, we show the effect of the electron-phonon scattering on the output characteristics of the device. A gate voltage $V_G = 0.4$ V is considered for these simulations. A channel length $L_{Ch} = 25$ nm is taken so as to show the phonon scattering contributions more clearly in the plot. We see for purely ballistic currents (shown in black) the drain current I_D for 1L-WSe_2 is higher than that for the 1L-MoS_2 channel. The optical phonon scattering (comprising of non-polar, TO and HP modes) contributes the highest in the degradation of drain current. This is followed by that due to the Frölich interaction and the acoustic phonon contributions (due to LA, TA and ZA modes).

The phonon scattering seems to degrade carrier transport in MoS_2 more than that in WSe_2 devices. The reason behind this is the stronger electron–phonon coupling in MoS_2, than the WSe_2 monolayer. This is quantitatively represented by the higher values of the deformation potentials (DP) for the various phonon modes for MoS_2 compared to WSe_2 as obtained by Kaasbjerg *et al.*[10] and Jin *et al.*[22] For the $L_{Ch} = 25$ nm device, the net reduction in I_D due to electron-phonon scattering effects are 18.6% for WSe_2, and 26.8% for 1L-MoS_2 devices. The variation of purely ballistic and the quasi-ballistic (inclusive of phonon scattering) ON currents with the device channel length is shown in Fig. 6. The ON currents are evaluated at $V_G = V_D = 0.4$ V. It is observed that the performance of the WSe_2 device is less impacted by phonon scattering, showing a ballisticity of

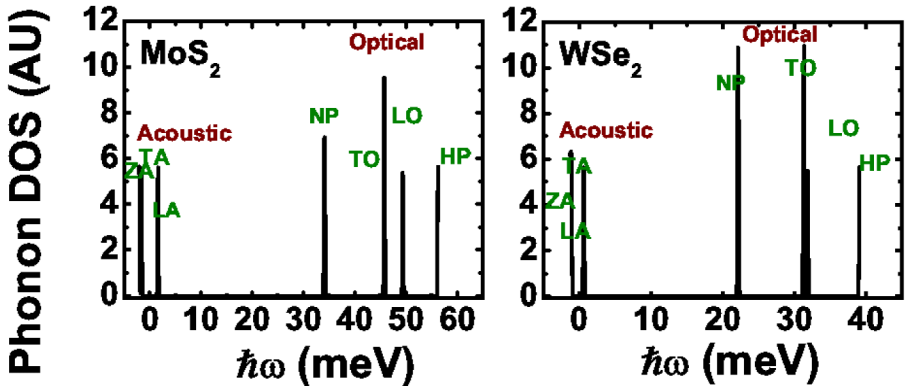

FIG. 4. The phonon density of states of single layer MoS_2 and WSe_2. The acoustic phonon branch consist of LA, TA and ZA modes, while the optical branch consists of NP, LO, TO and HP modes.

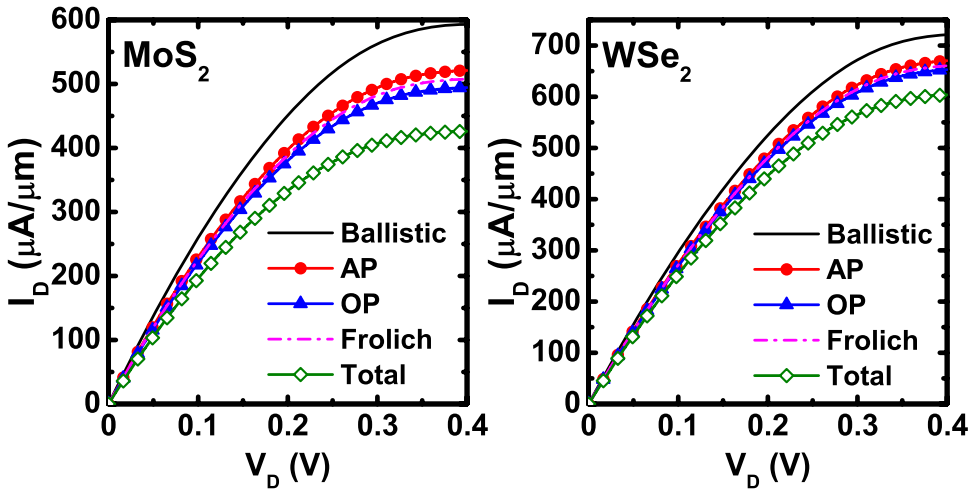

FIG. 5. The output characteristics of MoS_2 and WSe_2 n-MOSFET with $L_{Ch} = 25$ nm showing the contribution of different phonon modes to the scattering. Gate voltage $V_G = 0.4$ V.

83% for 1L-WSe_2 FET for channel length of 10 nm. Though 1L-MoS_2 FET of similar dimension shows a ballisticity of 75%. As the channel length increases, the electrons tend to encounter more number of scattering events and therefore the difference between the ballistic and quasi-ballistic currents tend to increase with the channel length. Here it must be mentioned that in our work we have included only the additional effect of electron-phonon scattering to the ballistic transport in MX_2 FET. Also we looked to focus our study on mostly short channel lengths as MX_2 as a channel material is essentially a candidate for post-Silicon sub decananometer CMOS technology. In experimentally fabricated devices the channel dimensions vary from several hundred nanometer[1,3] to even

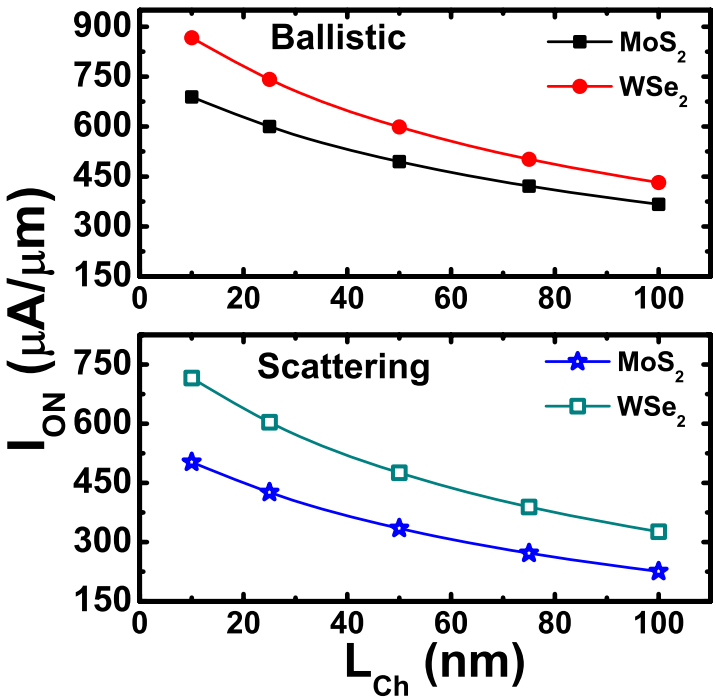

FIG. 6. The ballistic current and the current including scattering effects for the MoS_2 and WSe_2 n-MOSFET of varying channel lengths.

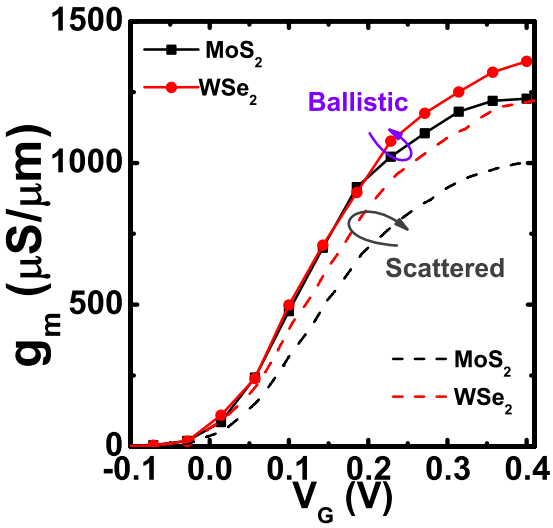

FIG. 7. Transconductance g_m vs gate voltage V_G plots for the ballistic and the quasi-ballistic case for a device of L_{Ch} = 25nm.

a few microns[2] with gate dielectric thickness of the order of few tens of nanometers.[1–3] In case of such fabricated devices, a vast number of non-idealities like surface roughness, defects and impurity scattering, intrinsic ripples in 2-D membranes, interface strain, processing related defects etc. apart from electron-phonon scattering, come into play. Owing to these effects there is a large difference between experimental results[1–3] and simulation studies that are being conducted by different groups.[4–6,12] For theoretical studies conducted for nanoscale FET of MX2 material, the ON currents are in the range of 500 $\mu A/\mu m$ for HfO_2 top gated Schottky barrier MoS2 SBFET of L_{Ch} = 15 nm.[4] For HfO_2 top-gated MOSFET in the scaling limit of L_{Ch} = 5 nm the simulated ON current is reported as 238 $\mu A/\mu m$ by Alam *et al.*[5] In this context our simulated results for L_{Ch} = 10 nm, top gated HfO_2 dielectric doped contact MoS2 MOFET shows ON current of 666 $\mu A/\mu m$ which is consistent with other theoretical results based on similar structures and device geometry and gating.[4]

The calculated values for the geometrical oxide capacitance C_{ox} is $0.22 fF/\mu m$, the channel quantum capacitance C_Q at $V_G = 0.4V$ is $0.16 fF/\mu m$ and the fringing capacitance C_f is $0.025 fF/\mu m$. The capacitances are calculated by the methods described by Alam *et al.*[5] For the 25 nm device, τ in the ballistic limit was calculated to be 0.67 ps for MoS_2 and 0.53 ps for WSe_2 FET. In case of MoS_2 FETs scattering seems to affect delay time much more severely than the WSe_2 FETs. As electron-phonon scattering is included the delay time increases significantly and the values increase to 0.91 ps and 0.64 ps for the MoS_2 and the WSe_2 FETs respectively.

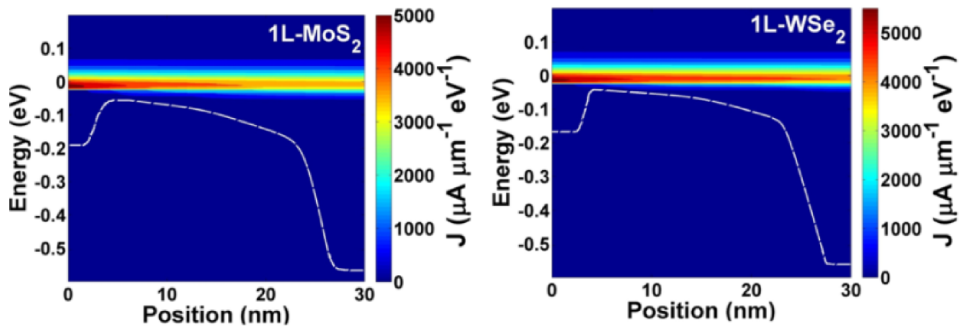

FIG. 8. The energy and position resolved current density and potential profile of single layer MoS_2 and WSe_2 n-MOSFET.

The transconductance (g_m) vs V_G characteristics in Fig. 7 of a 25nm device show a the ballistic values of g_m for the MX_2 are rather closely grouped together, while in the quasi-ballistic case the g_m-V_G curve are more spread out. This trend was earlier observed in the ON currents for ballistic and quasi-ballistic cases as well. The reason behind being the disparity in the amount of electron-phonon scattering among the two different MX_2 materials. The values of peak g_m for the MX_2 n-MOSFETs vary between 1226–1359$\mu S/\mu m$ for the ballistic cases.

The energy and position resolved current spectra is shown in Fig. 8. It is clear that the WSe_2 MOSFETs show a higher current density compared to the MoS_2 ones. Also the extension of the region of highest current density within the devices show that, for the 1L-WSe_2 this region (marked red in the colorbar) extends to a significant portion of the channel length. For 1L-MoS_2 the length of this region diminishes gradually due to higher degree of electron phonon scattering in the channel for those structures. In all the cases there is no evidence of direct tunnelling between the source and drain, as is expected for channel lengths of L_{Ch} = 25 nm.

IV. CONCLUSION

In this paper we study the effect of phonon scattering on the performance of monolayer (1L) MoS_2 and WSe_2 n-MOSFETs. Material properties of the channel are evaluated using the local density approximation (LDA) in density functional theory (DFT) using the Perdew–Zunger (PZ) exchange correlation. Thereafter using our in-house non-equilibrium Green's function (NEGF) simulator, we study the effect of phonon scattering on the performance of such devices. Individual contributions of the different phonon modes to the scattering and the effect of varying channel length of the device on performance parameters such as ON current, ballisticity, intrinsic delay time and transconductance are studied in detail. It is found that performance of WSe_2 devices are less impacted by phonon scattering compared to the MoS_2 counterparts.

ACKNOWLEDGMENTS

Dr. A. Sengupta thanks DST, Govt. of India, for the DST INSPIRE Faculty award. (Grant No. DST/INSPIRE/04/2013/000108).

[1] B. Radisavljevic, A. Radenovic, J. Brivio, V. Giacometti, and A. Kis, "Single-layer MoS_2 transistors," Nat. Nanotechnol. **6**(3), 147–150 (Mar. 2011).
[2] H. Liu and P. D. Ye, "MoS_2 Dual-Gate MOSFET With Atomic-Layer-Deposited Al_3O_3 as Top-Gate Dielectric," IEEE Electron Dev. Lett. **33**(4), 546–548 (Apr. 2012).
[3] H. Fang *et al.*, "High-Performance Single Layered WSe2 p-FETs with Chemically Doped Contacts," Nano Lett. **12**(7), 3788–3792 (Jun. 2012).
[4] Y. Yoon, K. Ganapathi, and S. Salahuddin, "How good can monolayer MoS_2 transistors be?," Nano Lett. **11**(9), 3768–3773 (Sep. 2011).
[5] K. Alam and R. K. Lake, "Monolayer MoS_2 Transistors beyond the technology road map," IEEE Trans. Electron Dev. **59**(12), 3250–3254 (2012).
[6] L. Liu, S. B. Kumar, Y. Ouyang, and J. Guo, "Performance limits of monolayer transition metal dichalcogenide transistors," IEEE Trans. Electron Dev. **58**(9), 3042–3047 (Sep. 2011).
[7] J. Na *et al.*, "Low-frequency noise in multilayer MoS_2 field-effect transistors: the effect of high-κ passivation," Nanoscale **6**(1), 433–441 (Oct. 2013).
[8] H. Li *et al.*, "Fabrication of Single- and Multilayer MoS_2 Film-Based Field-Effect Transistors for Sensing NO at Room Temperature," Small **8**(1), 63–67 (Jan. 2012).
[9] H. Wang *et al.*, "Integrated Circuits Based on Bilayer MoS2 Transistors," Nano Lett. **12**(9), 4674–4680 (Aug. 2012).
[10] K. Kaasbjerg, K. S. Thygesen, and K. W. Jacobsen, "Phonon-limited mobility in n-type single-layer MoS_2 from first principles," Phys. Rev. B **85**(11), 115317 (Mar. 2012).
[11] A. Molina-Sánchez and L. Wirtz, "Phonons in single-layer and few-layer MoS_2 and WS_2," Phys. Rev. B **84**(15), 115413 (Oct. 2011).
[12] L. Liu, S. B. Kumar, Y. Ouyang, and J. Guo, "On Monolayer MoS_2 Field-Effect Transistors at the Scaling Limit," IEEE Trans. Electron Dev. **60**(12), 4133–4139 (Dec. 2013).
[13] Atomistix ToolKit version 13.8.1, QuantumWise A/S (www.quantumwise.com).
[14] S. Bhattacharyya and A. K. Singh, "Semiconductor-metal transition in semiconducting bilayer sheets of transition-metal dichalcogenides," Phys. Rev. B **86**(7), 075454 (Aug. 2012).
[15] H. J. Monkhorst and J. D. Pack, "Special Points for Brillouin-zone integrations," Phys. Rev. B **13**(12), 5188–5192 (1976).
[16] W. Kohn and L. J. Sham, "Self-Consistent Equations Including Exchange and Correlation Effects," Phys. Rev. **140**(4A), A1133–A1138 (1965).

[17] [Online] https://wiki.fysik.dtu.dk/ase/ase/optimize.html for ASE code in BFGS optimization method.
[18] D. Nikonov, G. Bourianoff, P. Gargini, and H. Pal, Scattering in NEGF: Made simple [Online]. Available: https://nanohub.org/resources/7772.
[19] A. Sengupta, R. K. Ghosh, and S. Mahapatra, "Performance Analysis of Strained Monolayer MoS_2 MOSFET," IEEE Trans. Electron Dev. **60**(9), 2782–2787 (Sep. 2013).
[20] S. Datta, *Quantum Transport : Atom to Transistor* (Cambridge University Press, NY, 2005).
[21] S. Datta, "Nanoscale device modeling: the Greens function method," Superlattice and Microstructures **28**(4), 253–278 (Oct. 2000).
[22] Z. Jin, X. Li, J. T. Mullen, and K. W. Kim, "Intrinsic transport properties of electrons and holes in monolayer transition-metal dichalcogenides," Phys. Rev. B **90**(4), 045422(7) (Jul. 2014).